RSC Advances

PAPER

View Article Online
View Journal | View Issue

Cite this: *RSC Adv.*, 2018, **8**, 24500

Construction of 2D/2D layered g-C_3N_4/$Bi_{12}O_{17}Cl_2$ hybrid material with matched energy band structure and its improved photocatalytic performance†

Lei Shi, *[a] Weiwei Si,[a] Fangxiao Wang[c] and Wei Qi *[b]

Received 10th May 2018
Accepted 2nd July 2018

DOI: 10.1039/c8ra03981j

rsc.li/rsc-advances

A series of visible-light-induced 2D/2D layered g-C_3N_4/$Bi_{12}O_{17}Cl_2$ composite photocatalysts were successfully synthesized by a one step chemical precipitation method with g-C_3N_4, $BiCl_3$ and NaOH as the precursors at room temperature and characterized through XRD, FTIR, XPS, TEM, BET and UV-vis DRS measurements. The results of XRD, FTIR and XPS indicated that g-C_3N_4 has been introduced in the $Bi_{12}O_{17}Cl_2$ system. The TEM image demonstrated that there was strong surface-to-surface contact between 2D g-C_3N_4 layers and $Bi_{12}O_{17}Cl_2$ nanosheets, which contributed to a fast transfer of the interfacial electrons, leading to a high separation rate of photoinduced charge carriers in the g-C_3N_4/$Bi_{12}O_{17}Cl_2$ system. Rhodamine B was considered as the model pollutant to investigate the photocatalytic activity of the resultant samples. The g-C_3N_4/$Bi_{12}O_{17}Cl_2$ composite showed a clearly improved photocatalytic degradation capacity compared to bare g-C_3N_4 and $Bi_{12}O_{17}Cl_2$, which was ascribed to the interfacial contact between the 2D g-C_3N_4 layers and $Bi_{12}O_{17}Cl_2$ sheet with a matched energy band structure, promoting the photoinduced charges' efficient separation. Finally, combined with the results of the trapping experiment, ESR measurements and the band energy analysis, a reasonable photocatalytic mechanism over the 2D/2D layered g-C_3N_4/$Bi_{12}O_{17}Cl_2$ composite was proposed.

1. Introduction

The photocatalytic technique is considered as one of the applied prospect strategies to rationally utilize solar energy for resolving energy and environmental problems, and has drawn extensive attention in the field of green chemistry and materials science during the past few decades. Conventional semiconductor materials, including TiO_2, ZnO, SnO_2, *etc.*, have showed admirable photocatalytic properties for splitting water to produce H_2 and degrading all kinds of pollutants under ultraviolet (UV) irradiation.[1–3] Nevertheless, in view of the sufficient utilization of the abundant solar energy, it is essential to exploit visible-light-induced and efficient semiconductor photocatalysts.

Recently, bismuth oxyhalide (BiOX, X = Cl, Br, I) has attracted more and more attention in photocatalytic degradation of environmental pollutants and energy conversion *etc.*[4–7] Due to the unique layered structure and internal static electric fields perpendicular to each layer, BiOX could effectively separate photogenerated electron–hole pairs, achieving enhanced photocatalytic performance.[8] Among these BiOX materials, BiOCl has been sufficiently researched,[9,10] nevertheless, the relatively wide energy band limits its photocatalytic efficiency. In order to improve the visible light induced photocatalytic performance of BiOCl, some bismuth oxychlorides with non-stoichiometric ratios were developed, such as Bi_3O_4Cl,[11] $Bi_{12}O_{15}Cl_6$ (ref. 12) and $Bi_{24}O_{31}Cl_{10}$,[13] *etc.*, which have been proposed and intensively studied in the field of photocatalysis. Among these materials, $Bi_{12}O_{17}Cl_2$ has revealed superb visible-light photocatalytic properties in selective oxidation and degradation of various organic pollutants.[14,15] Nevertheless, its photocatalytic performance was still limited by the low separation rate of photogenerated electrons and holes. Hence, it is interesting to improve its photocatalytic properties through some modified method. For this kind of 2D sheet material, it is an effective method to fabricate interfaces through surface to surface *via* introducing other two-dimensional (2D) layered semiconductor components, which contribute to promote the charge separation.

As one of the representative layered materials, graphitic carbon nitride (g-C_3N_4), has shown several advantages as

[a]College of Chemistry, Chemical Engineering and Environmental Engineering, Liaoning Shihua University, Fushun 113001, China. E-mail: shilei_hit@qq.com

[b]Shenyang National Laboratory for Materials Science, Institute of Metal Research, Chinese Academy of Sciences, Shenyang 110016, China. E-mail: wqi@imr.ac.cn; Tel: +86-02456861842

[c]College of Chemistry, Chemical Engineering and Material Science, Shandong Normal University, Jinan 250014, China

† Electronic supplementary information (ESI) available. See DOI: 10.1039/c8ra03981j

photocatalysts, such as low-cost, high thermal and chemical stability *etc.*[16–18] In addition, the appropriate valence and conduction band position makes the g-C_3N_4 compound be widely applied in some photocatalytic processes. Several individual research groups have reported that various g-C_3N_4-based composite photocatalysts have been successfully synthesized and utilized, such as MoS_2/g-C_3N_4,[19] BiOCl/C_3N_4,[20] g-C_3N_4/Ag_3PO_4,[21] g-C_3N_4/$BiPO_4$,[22] CdS/g-C_3N_4,[23] SnO_2/g-C_3N_4,[24] $Bi_2O_2CO_3$/g-C_3N_4,[25] g-C_3N_4/Bi_2MoO_6,[26] g-C_3N_4/ZnO,[27] BiOBr/g-C_3N_4,[28] g-C_3N_4/$Bi_4O_5I_2$,[29] and so on. The general concept for the catalyst design among these research work is the rational combination of the two type components yielding hybrid materials with accurate energy band and relatively high photocatalytic performance. Therefore, it seems to be ideal that the combination of g-C_3N_4 with $Bi_{12}O_{17}Cl_2$ might improve their photocatalytic performance. Zhou *et al.* prepared the carbon-doped carbon nitride/$Bi_{12}O_{17}Cl_2$ (CCN/$Bi_{12}O_{17}Cl_2$), which had superior photocatalytic performance for degrading antibiotic tetracycline.[30] However, this work involved the solvothermal preparation of $Bi_{12}O_{17}Cl_2$ and ultrasonic combination of CCN/$Bi_{12}O_{17}Cl_2$, preparation process was multi-step. Hence, it is necessary to develop the facile strategy for preparing carbon nitride/$Bi_{12}O_{17}Cl_2$ composite.

Therefore, in the present study, we have developed 2D/2D layered g-C_3N_4/$Bi_{12}O_{17}Cl_2$ composite materials by one step chemical precipitation method at room temperature. The chemical structure, composition, morphology and optical property of the synthesized g-C_3N_4/$Bi_{12}O_{17}Cl_2$ composites were thoroughly characterized. The related results indicated that g-C_3N_4 and $Bi_{12}O_{17}Cl_2$ matched complementary potentials of conduction band and valence band in g-C_3N_4/$Bi_{12}O_{17}Cl_2$ composite, which could effectively separate the photogenerated electron–hole pairs, resulting that g-C_3N_4/$Bi_{12}O_{17}Cl_2$ heterojunctions revealed excellent photocatalytic activity and recycling stability for degrading rhodamine B (RhB). Finally, the reasonable mechanism for the improved photocatalytic capacity over g-C_3N_4/$Bi_{12}O_{17}Cl_2$ composite was proposed.

2. Experimental section

2.1 Preparation of the photo-catalyst

g-C_3N_4 was obtained by pyrolysis of urea (30 g) at 550 °C for 2 h in an oven.

g-C_3N_4/$Bi_{12}O_{17}Cl_2$ composite was prepared at room temperature as following procedures. A given amount of g-C_3N_4 (9.5, 28.5, 47.5 and 66.6 mg) and 4 mmol $BiCl_3$ were dissolved in 20 mL ethanol under continuous stirring for 30 min, and the pH of solution was about 2. 20 mL of distilled water containing 24 mmol NaOH was added dropwisely into above mixture, then the solution vigorously stirred for 120 min with stirred rate 150rpm, and the pH of solution become to 14, the obtained product was filtered, washed with distilled water and ethanol, and dried at 60 °C in a oven for 12 h. In prepared process of samples, the system did not proceed exothermic. On the basis of the theoretical mass ratio of g-C_3N_4 and $Bi_{12}O_{17}Cl_2$, the as-made composites were denoted as g-C_3N_4/$Bi_{12}O_{17}Cl_2$ (1 wt%), g-C_3N_4/$Bi_{12}O_{17}Cl_2$ (3 wt%), g-C_3N_4/$Bi_{12}O_{17}Cl_2$ (5 wt%) and g-C_3N_4/$Bi_{12}O_{17}Cl_2$ (7 wt%), respectively. For comparison, pure $Bi_{12}O_{17}Cl_2$ was obtained according to above method without g-C_3N_4, and similar method has been reported in previous literatures.[31,32] In addition, N-doped TiO_2 (N–TiO_2) was prepared by heating with TiO_2 (P25) and urea as the precursor according to previous reports.[33,34] Carbon nanotubes modified $Bi_{12}O_{17}Cl_2$ composite (CNTs/$Bi_{12}O_{17}Cl_2$) and CCN/$Bi_{12}O_{17}Cl_2$ were prepared according to previous reports.[30,35]

2.2 Characterizations

The X-ray diffraction (XRD) patterns of all as-made samples were measured by an X-ray diffractometer (Bruker D8 Advance). Fourier transform infrared spectra (FTIR) of all as-prepared samples were detected by Thermo Fisher Scientific IS10. The X-ray photoelectron spectroscopy (XPS) of g-C_3N_4/$Bi_{12}O_{17}Cl_2$ (3 wt%) composite was recorded on Thermo Fisher Scientific Escalab 250. The microtopographies of g-C_3N_4, $Bi_{12}O_{17}Cl_2$ and g-C_3N_4/$Bi_{12}O_{17}Cl_2$ (3 wt%) composite were observed using JEM-2100F transmission electron microscope (TEM). The UV-vis diffuse reflectance spectra (DRS) of as-made samples were collected by an UV-vis spectrometer (Agilent Cary 5000). BET surface areas of all as-made samples were collected using a Micromeritics Tristar 3020 analyzer. Samples were outgassed at 150 °C for 12 h prior to measurements. Transient photocurrent properties of g-C_3N_4, $Bi_{12}O_{17}Cl_2$ and g-C_3N_4/$Bi_{12}O_{17}Cl_2$ (3 wt%) were measured by a CHI760 electrochemical system (China) in a three-electrode quartz cells. Pt wire was the counter electrode, and the saturated calomel electrode was the reference electrode. The sample films coated on ITO glasses were applied as the working electrode was. A 300 W Xe lamp with 400 nm filters provided the light source, and the electrolyte was 0.1 M Na_2SO_4. The total organic carbon (TOC) assays were investigated by using a Shimadzu TOC-VCPH analyzer.

2.3 Photocatalytic testing

The photocatalytic property of the resultant sample was evaluated using degradation of RhB or methyl orange (MO) as a model reaction, which was performed under visible-light irradiation. A 300 W Xe lamp with a 400 nm cutoff filter was used for the visible-light source. 30 mg resultant sample was dispersed into 50 mL 5 mg L^{-1} RhB or 10 mg L^{-1} MO solution and the solution was stirred in dark for 1 h to reach the adsorption–desorption equilibrium. About a certain volume solutions were collected at every given time interval under irradiation, and the catalyst was removed *via* centrifugation (10 000 rpm, 3 min). The concentration of RhB or MO was detected through a UV-vis spectrophotometer at the wavelength of 552 or 464 nm.

3. Results and discussions

Fig. 1 shows the XRD patterns of all the resultant samples. For pure $Bi_{12}O_{17}Cl_2$, there are some diffraction peaks corresponding to the tetragonal $Bi_{12}O_{17}Cl_2$ (JCPDS No. 37-0702),[36] including (113), (115), (117), (0012), (200), (220) and (317). g-C_3N_4 compounds have two distinct diffraction peaks at 27.4°

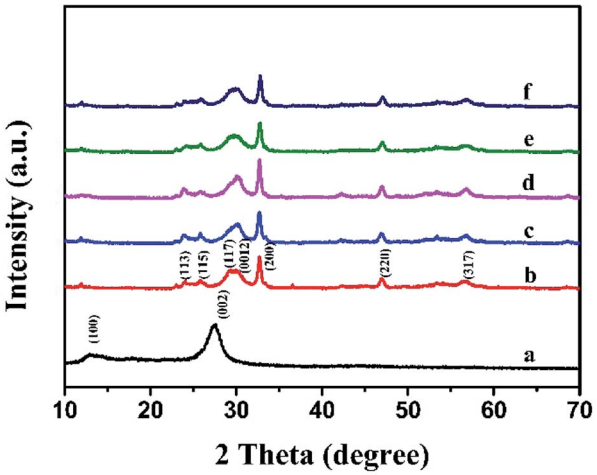

Fig. 1 The XRD patterns of (a) g-C_3N_4, (b) $Bi_{12}O_{17}Cl_2$, (c) g-C_3N_4/$Bi_{12}O_{17}Cl_2$ (1 wt%), (d) g-C_3N_4/$Bi_{12}O_{17}Cl_2$ (3 wt%), (e) g-C_3N_4/$Bi_{12}O_{17}Cl_2$ (5 wt%) and (f) g-C_3N_4/$Bi_{12}O_{17}Cl_2$ (7 wt%).

and 13.1°, which were indexed to the (002) and (100) planes of hexagonal g-C_3N_4 (JCPDS 87-1526),[37] and the two diffraction peaks were in good agreement with the previous report.[38–40] However, no diffraction peaks belonged to g-C_3N_4 were found in as-prepared g-C_3N_4/$Bi_{12}O_{17}Cl_2$ composite, which might be attributed to the low contents of g-C_3N_4 or their relatively high dispersions. Hence, to prove that g-C_3N_4 was introduced in the $Bi_{12}O_{17}Cl_2$ system, the FTIR, XPS and TEM were also carried out.

Firstly, FTIR analysis was investigated. Fig. 2 presents the FTIR results of the pure g-C_3N_4, $Bi_{12}O_{17}Cl_2$ and a series of g-C_3N_4/$Bi_{12}O_{17}Cl_2$ composites. For pure g-C_3N_4, there were some vibration bands at 810 cm^{-1} and the scope of 1200–1650 cm^{-1}, which could be assigned as the typical breathing mode of *s*-triazine and stretching vibration modes of heptazine heterocyclic ring in g-C_3N_4.[41] Meanwhile, these characteristic IR signals could be also observed for as-made g-C_3N_4/$Bi_{12}O_{17}Cl_2$ composites, suggesting that the 2D g-C_3N_4 has successfully incorporated with the $Bi_{12}O_{17}Cl_2$ nano-material, verifying that g-C_3N_4/$Bi_{12}O_{17}Cl_2$ photocatalyst has been synthesised.

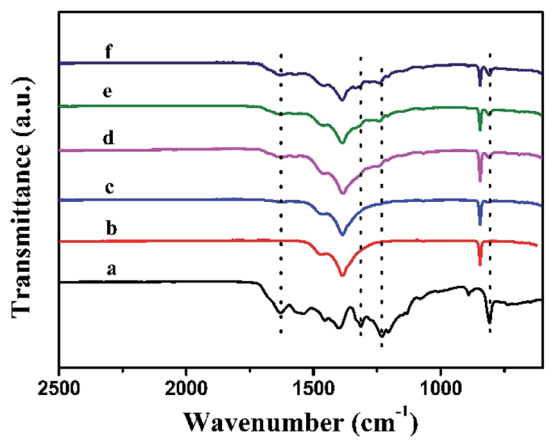

Fig. 2 The FTIR spectra of (a) g-C_3N_4, (b) $Bi_{12}O_{17}Cl_2$, (c) g-C_3N_4/$Bi_{12}O_{17}Cl_2$ (1 wt%), (d) g-C_3N_4/$Bi_{12}O_{17}Cl_2$ (3 wt%), (e) g-C_3N_4/$Bi_{12}O_{17}Cl_2$ (5 wt%) and (f) g-C_3N_4/$Bi_{12}O_{17}Cl_2$ (7 wt%).

Fig. 3 shows the XPS survey and the corresponding Bi 4f, Cl 2p, O 1s, C 1s and N 1s high-resolution spectra for g-C_3N_4/$Bi_{12}O_{17}Cl_2$ (3 wt%) composite. The XPS survey spectra (Fig. 3A) indicates that the elements of Bi, Cl, O, C and N exist in the g-C_3N_4/$Bi_{12}O_{17}Cl_2$ composite. In the Bi 4f high-resolution spectra (Fig. 3B), the peaks at 159.1 and 164.4 eV could be assigned as the Bi $4f_{7/2}$ and Bi $4f_{5/2}$, respectively.[42] For the Cl 2p spectrum in Fig. 3C, the signal is deconvoluted into two peaks at 197.9 and 199.6 eV, attributed to Cl $2p_{3/2}$ and Cl $2p_{1/2}$ signals, respectively, deriving from the Cl^-.[43] In Fig. 3D, the O 1s spectrum is deconvoluted into two peaks. The former belonged to the Bi–O bonds in $[Bi_2O_2]^{2+}$ slabs, and the latter might correspond to the surface adsorbed hydroxy groups.[44] For C 1s signal in Fig. 3E, the peaks at 284.6 and 288.7 eV could be ascribed to carbon atoms and the sp^2 C=N bonded, respectively.[45] The N 1s spectrum (Fig. 3F) is deconvoluted into three peaks with binding energies at 398.7, 399.8 and 401.3 eV, respectively. The peak at 398.8 eV is typically attributed to C–N=C. The two peaks at 399.8 and 401.4 eV could be assigned to N–$(C)_3$ and N–H, respectively.[46] The above results revealed the surface property and chemical composition of the g-C_3N_4/$Bi_{12}O_{17}Cl_2$ composite and further confirmed the successful combination of g-C_3N_4 and $Bi_{12}O_{17}Cl_2$ species, which agrees with FTIR results.

The morphology features of g-C_3N_4/$Bi_{12}O_{17}Cl_2$ composite is revealed *via* TEM measurements. As can be shown in Fig. 4A, pure g-C_3N_4 exhibits its typical 2D nanosheet morphology, and there are some pores on the surface. For pure $Bi_{12}O_{17}Cl_2$ seen in Fig. 4B, the typical 2D nanosheets are observed, and the surface of them are normally smooth. Fig. 4C gives the corresponding TEM image of the g-C_3N_4/$Bi_{12}O_{17}Cl_2$ composite. $Bi_{12}O_{17}Cl_2$ nanosheets were loaded on the surface g-C_3N_4 *via* surface-to-surface contact, which could favor the charges transfer between these two components. Moreover, the HRTEM image in Fig. 4D indicates that the lattice fringe spacing of 0.272 and 0.306 nm could be observed respectively, attributing to the (2 0 0) and (1 1 7) plane of $Bi_{12}O_{17}Cl_2$ species, and there is a close combination and the formation of the interface between $Bi_{12}O_{17}Cl_2$ and g-C_3N_4, which might benefit the transfer of the photogenerated electrons, leading to the improved photocatalytic property. TEM results suggest the successful hybridization of g-C_3N_4 and $Bi_{12}O_{17}Cl_2$. The layered 2D structure of the two components are well maintained, and the formation of the interfaces between the two species may facilitate the electron transfer process.

BET surface area of the as-prepared g-C_3N_4, $Bi_{12}O_{17}Cl_2$, g-C_3N_4/$Bi_{12}O_{17}Cl_2$ (1 wt%), g-C_3N_4/$Bi_{12}O_{17}Cl_2$ (3 wt%), g-C_3N_4/$Bi_{12}O_{17}Cl_2$ (5 wt%) and g-C_3N_4/$Bi_{12}O_{17}Cl_2$ (7 wt%) are 45.8, 25.5, 26.7, 28.3, 30 and 31.6 $m^2\ g^{-1}$, respectively. The combination of g-C_3N_4 could increase the surface area of the composites, which could contribute to improve photocatalytic performance of the composite.

UV-vis diffuse reflectance spectra of g-C_3N_4, $Bi_{12}O_{17}Cl_2$, g-C_3N_4/$Bi_{12}O_{17}Cl_2$ (1 wt%), g-C_3N_4/$Bi_{12}O_{17}Cl_2$ (3 wt%), g-C_3N_4/$Bi_{12}O_{17}Cl_2$ (5 wt%) and g-C_3N_4/$Bi_{12}O_{17}Cl_2$ (7 wt%) were also measured to show their light adsorption ability. As illustrated from Fig. 5A, for pure $Bi_{12}O_{17}Cl_2$, the adsorption edge is approximate 500 nm, showing excellent photo-absorptions

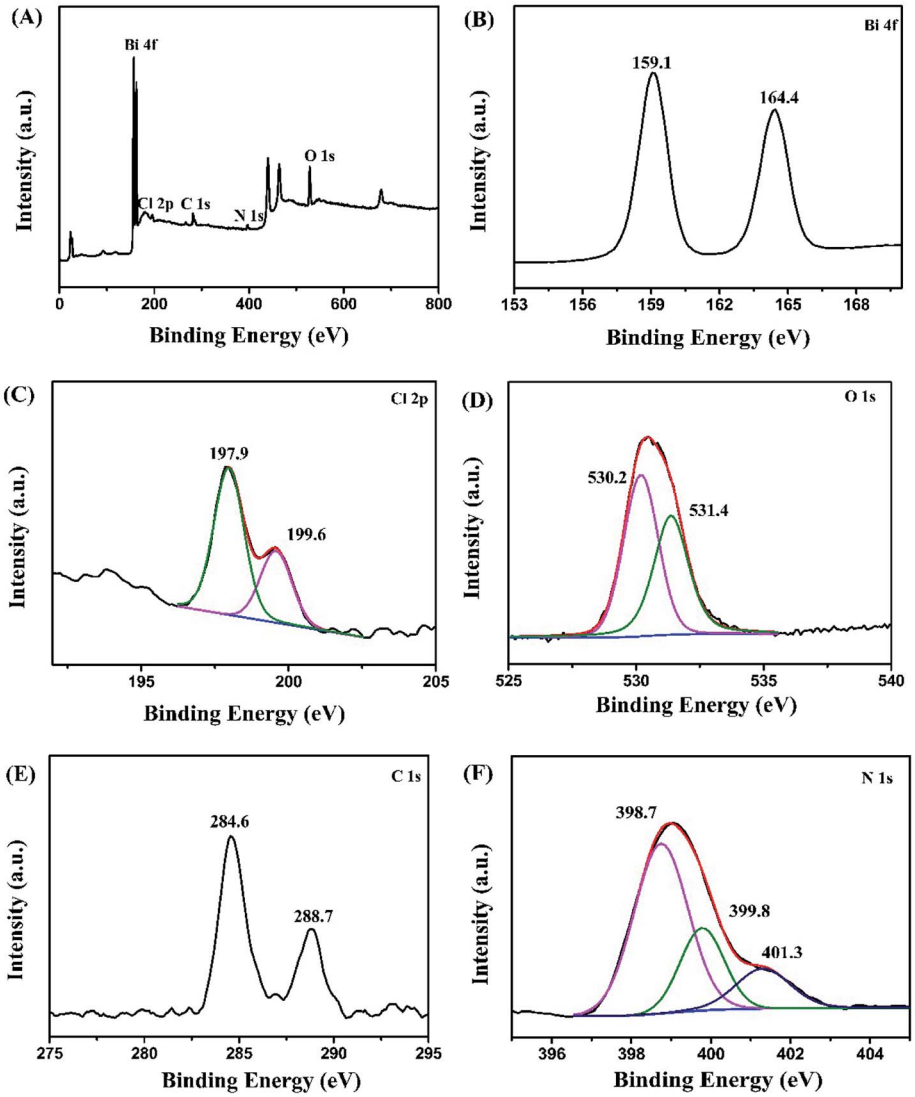

Fig. 3 XPS spectra of g-C_3N_4/$Bi_{12}O_{17}Cl_2$ (3 wt%) composite: (A) survey spectra, (B) Bi 4f, (C) Cl 2p, (D) O 1s, (E) C 1s and (F) N 1s.

ability. g-C_3N_4 displays photoresponse from ultraviolet to visible light region, and its adsorption edge is at approximate 460 nm. After the cooperation of $Bi_{12}O_{17}Cl_2$ and g-C_3N_4, a series of g-C_3N_4/$Bi_{12}O_{17}Cl_2$ composites exhibit a similar absorption ability as $Bi_{12}O_{17}Cl_2$, indicating that the introduction of g-C_3N_4 has little effect on the light absorption of $Bi_{12}O_{17}Cl_2$. In addition, the band gap energies of the as-prepared g-C_3N_4 and $Bi_{12}O_{17}Cl_2$ are obtained *via* following equation.[47,48]

$$\alpha h\nu = A(h\nu - E_g)^{n/2} \quad (1)$$

where α, h, ν, E_g and A are the absorption coefficiency, Planck constant, light frequency, band gap energy, and a constant, respectively. As illustrated in Fig. 5B, the band gap of g-C_3N_4 and $Bi_{12}O_{17}Cl_2$ are 2.65 eV and 2.48 eV, respectively.

Photocurrent measurement is an effective method for estimating the separation efficiency of photoinduced electrons and holes. Currently, the higher photocurrent intensity indicates the better separated efficiency of photoinduced electrons and holes. As seen in Fig. 6, the visible light irradiation could result pure $Bi_{12}O_{17}Cl_2$, g-C_3N_4 and g-C_3N_4 modified $Bi_{12}O_{17}Cl_2$ samples to create photocurrent signals. Clearly, the photocurrent intensity of g-C_3N_4/$Bi_{12}O_{17}Cl_2$ (3 wt%) composite is higher than that of pure $Bi_{12}O_{17}Cl_2$ and g-C_3N_4, meaning that the introduction of g-C_3N_4 modifier could promote in the effective separation of photogenerated electron–hole pairs.

The visible-light photocatalytic activities of the as-prepared samples were estimated by liquid phase degradation of pollutant, and RhB was chose as a model pollutant. As seen in Fig. 7A, the blank experiment revealed that RhB could be hardly decomposed without any photo-catalysts. Single g-C_3N_4 or $Bi_{12}O_{17}Cl_2$ was employed as photocatalysts, about 76% or 83% of RhB was degraded respectively. After their coordination, the resultant g-C_3N_4/$Bi_{12}O_{17}Cl_2$ composites revealed obviously enhanced photocatalytic performance under the same condition. In addition, the photocatalytic performance of CNTs/$Bi_{12}O_{17}Cl_2$, N–TiO_2 and CCN/$Bi_{12}O_{17}Cl_2$ were also detected as

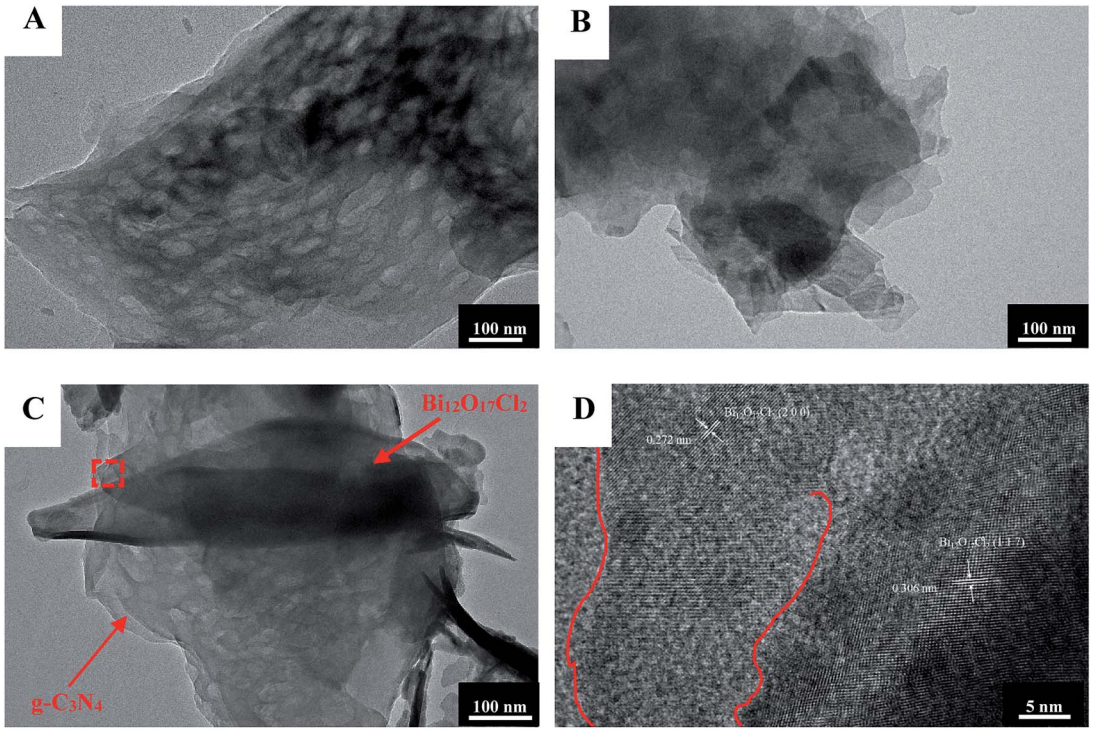

Fig. 4 The TEM images of (A) pure g-C_3N_4, (B) $Bi_{12}O_{17}Cl_2$ and (C and D) g-C_3N_4/$Bi_{12}O_{17}Cl_2$ (3 wt%) composite.

the compared samples and the related results were shown in Fig. 7A. Clearly, their photocatalytic activities were worse than that of g-C_3N_4/$Bi_{12}O_{17}Cl_2$ (3 wt%) nanocomposite, meaning that as-prepared g-C_3N_4/$Bi_{12}O_{17}Cl_2$ nanocomposite was an effective photocatalyst. In addition, the photodegradation of various concentration RhB (10 mg L^{-1}, 15 mg L^{-1} and 20 mg L^{-1}) over g-C_3N_4/$Bi_{12}O_{17}Cl_2$ (3 wt%) nanocomposite was carried out. As shown in Fig. S1,† RhB was still degraded even if the concentration of RhB increased. And the TOC of RhB solution over as-prepare g-C_3N_4/$Bi_{12}O_{17}Cl_2$ (3 wt%) after photodegradation 1 h was detected in Fig. S2,† the related result indicated that the TOC decreased 90%, which implied that g-C_3N_4/$Bi_{12}O_{17}Cl_2$ nanocomposite exhibited excellent photocatalytic activity for removing pollutant. In addition, as a the azo reactive dye, methyl orange (10 mg L^{-1}) was also chose as the model pollutant to access the photocatalytic performance of g-C_3N_4/$Bi_{12}O_{17}Cl_2$ (3 wt%) nanocomposite. It could be seen that MO can be degraded 85% over g-C_3N_4/$Bi_{12}O_{17}Cl_2$ (3 wt%) in the 120 min in Fig. S3.†

Following, in Fig. 7B, a pseudo-first-order reaction kinetic model for the photo-catalytic degradation of RhB could be described as the following rate equation:

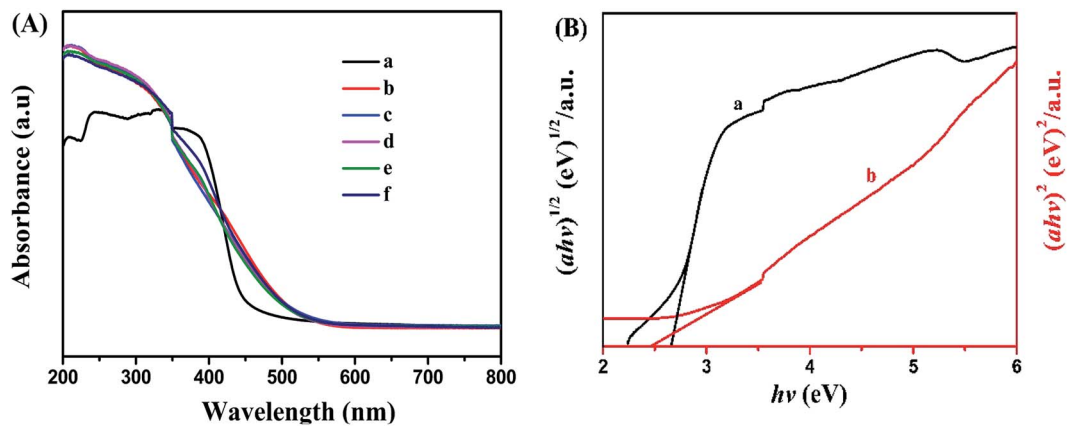

Fig. 5 (A) UV-vis diffuse reflectance spectra of (a) g-C_3N_4, (b) $Bi_{12}O_{17}Cl_2$, (c) g-C_3N_4/$Bi_{12}O_{17}Cl_2$ (1 wt%), (d) g-C_3N_4/$Bi_{12}O_{17}Cl_2$ (3 wt%), (e) g-C_3N_4/$Bi_{12}O_{17}Cl_2$ (5 wt%) and (f) g-C_3N_4/$Bi_{12}O_{17}Cl_2$ (7 wt%); (B) plot of $(\alpha hv)^{1/2}$ *versus* hv for the E_g of (a) g-C_3N_4 and the plot of $(\alpha hv)^2$ *versus* hv for the E_g of (b) $Bi_{12}O_{17}Cl_2$.

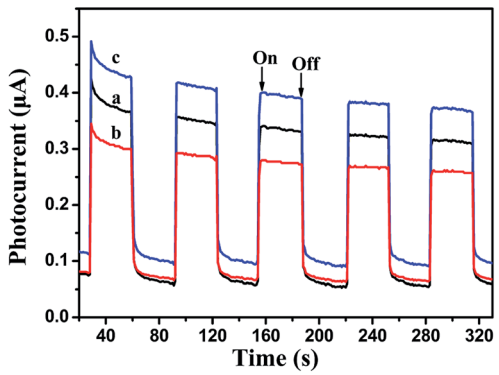

Fig. 6 Transient photocurrent property of (a) pure $Bi_{12}O_{17}Cl_2$, (b) g-C_3N_4 and (c) g-C_3N_4/$Bi_{12}O_{17}Cl_2$ (3 wt%).

$$\ln(C_0/C) = kt \quad (2)$$

where C_0 is the absorption equilibrium concentration of dye solution. C represents the concentration of the remaining dye solution at given reaction time (t), and k is the degraded rate constant. As seen in Fig. 7C, resultant g-C_3N_4/$Bi_{12}O_{17}Cl_2$ (3 wt%) composite showed the highest rate constant (0.353 min^{-1}), which was about 4.5 times higher than that of g-C_3N_4 (0.078 min^{-1}), and 3.4 times higher than that of pure $Bi_{12}O_{17}Cl_2$ (0.102 min^{-1}), and higher than that of CNTs/$Bi_{12}O_{17}Cl_2$ (0.138 min^{-1}), N–TiO_2 (0.0179 min^{-1}) and CCN/$Bi_{12}O_{17}Cl_2$ (0.153 min^{-1}). With further increasing the g-C_3N_4 amount, the photocatalytic performance would decrease, meaning that the content of g-C_3N_4 was important for the optimal photocatalytic activity.

Moreover, the sustainable used ability of a photocatalyst is a significant factor for its assessment and potential applications. Hence, the recycling runs for the photocatalytic degradation of RhB over g-C_3N_4/$Bi_{12}O_{17}Cl_2$ (3 wt%) composite were performed to evaluate its photocatalytic stability. After reaction was over, g-C_3N_4/$Bi_{12}O_{17}Cl_2$ (3 wt%) composite was separated, and washed with abundant water and ethanol, then dried at 60 °C, subsequently, dispersed in another fresh 5 mg L^{-1} RhB aqueous solution for next run. The experimental result was presented in Fig. 7D. It could be found that the photocatalytic activity remained nearly 85% of the first run after five times recycling, indicative of the acceptable stability of g-C_3N_4/$Bi_{12}O_{17}Cl_2$ catalysts.

Generally, several active species, such as electrons (e^-), holes (h^+), superoxide radicals ($^{\bullet}O_2^-$) and hydroxyl radicals ($^{\bullet}OH$), *etc.*, are generated in the process of photo-degradation under light irradiation in the presence of photo-catalysts. To identify and quantify the dominating reactive species in the photo-degradation process over g-C_3N_4/$Bi_{12}O_{17}Cl_2$ composite and propose the reasonable photocatalytic mechanism, reactive specie trapping experiments were performed. Here, ascorbic acid (AA, 1 mmol L^{-1}), ethylenediaminetetraacetic acid disodium salt (EDTA-2Na, 1 mmol L^{-1}) and methanol (1 mmol L^{-1})

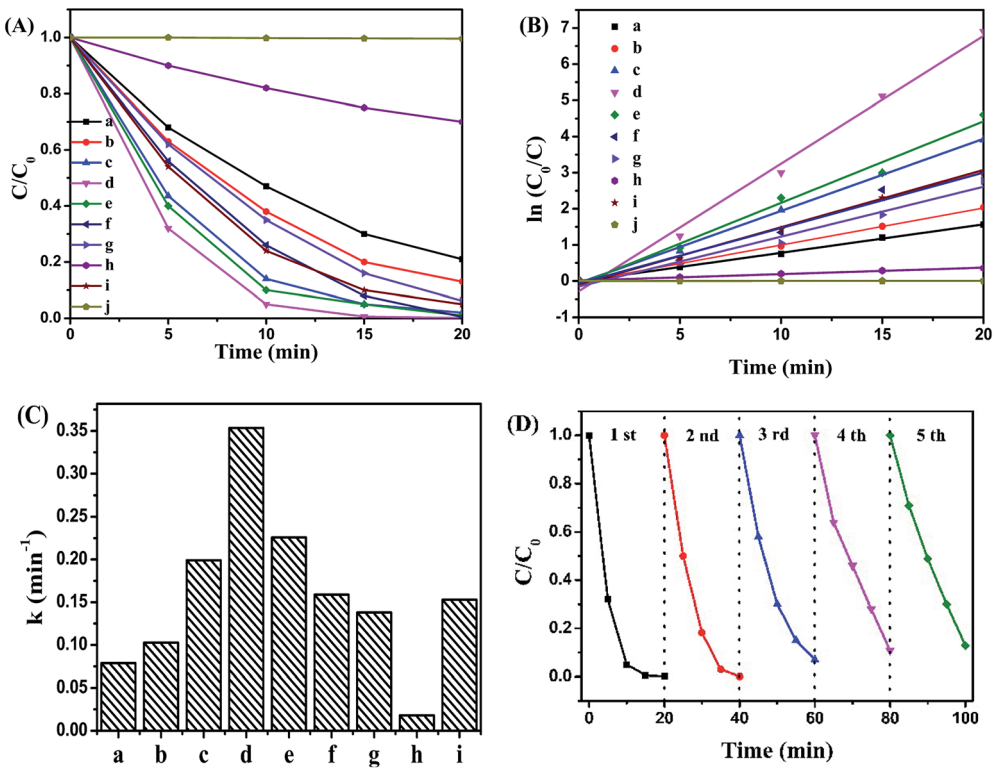

Fig. 7 (A) The photodegradation curves of RhB; (B) first-order kinetic plots for the photodegradation of RhB; (C) the rate constant of various samples; (D) recycling experiments for photodegrading RhB over g-C_3N_4/$Bi_{12}O_{17}Cl_2$ (3 wt%) composite. (a) g-C_3N_4, (b) pure $Bi_{12}O_{17}Cl_2$, (c) g-C_3N_4/$Bi_{12}O_{17}Cl_2$ (1 wt%), (d) g-C_3N_4/$Bi_{12}O_{17}Cl_2$ (3 wt%), (e) g-C_3N_4/$Bi_{12}O_{17}Cl_2$ (5 wt%), (f) g-C_3N_4/$Bi_{12}O_{17}Cl_2$ (7 wt%), (g) CNTs/$Bi_{12}O_{17}Cl_2$, (h) N–TiO_2, (i) CCN/$Bi_{12}O_{17}Cl_2$ and (j) blank.

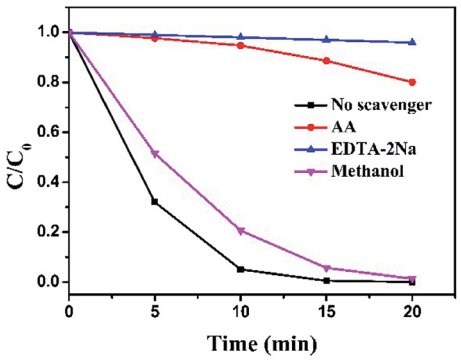

Fig. 8 Active species trapping experiments over g-C_3N_4/$Bi_{12}O_{17}Cl_2$ (3 wt%) composite.

were respectively added into photocatalytic system, which served as scavenger to quench $^{\bullet}O_2^-$, h^+ and $^{\bullet}OH$.[49–52] As shown in Fig. 8, after AA and EDTA-2Na were added into the photocatalytic reaction system, respectively, it was clearly observed that the photodegraded activity of the g-C_3N_4/$Bi_{12}O_{17}Cl_2$ composite was sharply declined, meaning that $^{\bullet}O_2^-$ and h^+ radical were the key active species in this reaction. On the contrast, the introduction of methanol only resulted in a small inhibition for the photo-degradation of RhB, indicating that $^{\bullet}OH$ radical may have limited activity in the present photocatalytic reaction.

To further identify the radical species during the photocatalytic process, electron spin resonance (ESR) spectra technique was also applied using 5,5-dimethyl-1-pyrroline-N-oxide (DMPO) as scavengers in the presence of methanol (forming DMPO-$\cdot O_2^-$) and deionized water (forming DMPO-$^{\bullet}OH$), respectively, on a Germany A300-10/12 spectrometer. As represented in Fig. 9, when the system was in dark, no any signals could be detected. After visible light was irradiated for several minutes, evident signals belonging to $\cdot O_2^-$ and $\cdot OH$ radicals were observed, which proved the generation of $\cdot O_2^-$ and $\cdot OH$ radicals.

To better explain the photocatalytic mechanism and the enhanced activity of g-C_3N_4/$Bi_{12}O_{17}Cl_2$ hybrid materials, the valence band (VB) structure of g-C_3N_4 and $Bi_{12}O_{17}Cl_2$ were measured in Fig. 10. It could be clearly observed that the VB maxima of g-C_3N_4 and $Bi_{12}O_{17}Cl_2$ located at 1.85 and 1.39 eV, respectively. Hence, the conduction band (CB) potentials (E_{CB}) of g-C_3N_4 and $Bi_{12}O_{17}Cl_2$ could be calculated according to eqn (3).[53]

$$E_{CB} = E_{VB} - E_g \quad (3)$$

wherein E_{VB} and E_g are the valence band edge potentials and band gap energy of the semiconductors, respectively. The E_g of g-C_3N_4 and $Bi_{12}O_{17}Cl_2$ is 2.65 and 2.48 eV, respectively (Fig. 5B). As a result, the E_{VB} and E_{CB} of g-C_3N_4 are calculated to be 1.85 and −0.80 eV, and the E_{VB} and E_{CB} of $Bi_{12}O_{17}Cl_2$ are 1.39 and −1.09 eV, respectively. Clearly, g-C_3N_4 and $Bi_{12}O_{17}Cl_2$ possessed complementary potentials of conduction band and valence band, which could effectively separate the photo-generated electron–hole pairs.

Therefore, combining with the above experimental results, Fig. 11 illustrates a reasonable photocatalytic mechanism for degrading organic pollutants over g-C_3N_4/$Bi_{12}O_{17}Cl_2$ composite. Electrons (e^-) and holes (h^+) were easily generated after g-C_3N_4/$Bi_{12}O_{17}Cl_2$ composite was irradiated by visible light. The e^- in the CB of $Bi_{12}O_{17}Cl_2$ could transfer to the CB of g-C_3N_4, because the CB and VB of g-C_3N_4 lie below those of $Bi_{12}O_{17}Cl_2$, at the same time, h^+ left in the VB of g-C_3N_4 would transfer to the VB of $Bi_{12}O_{17}Cl_2$. Then e^- could reduce the adsorbed O_2 to form superoxide radicals ($^{\bullet}O_2^-$), which might react with H_2O to further generate the active $^{\bullet}OH$ species.[54,55] Because the VB level of $Bi_{12}O_{17}Cl_2$ was less positive than the standard redox potential of $^{\bullet}OH/H_2O$ (2.68 eV *vs.* SHE),[56] abundant h^+ in the VB of $Bi_{12}O_{17}Cl_2$ would be directly involved into the degradation of pollutants. This result might explain why $^{\bullet}OH$ radical had limited influence on the photodegraded efficiency of pollutant. Finally, the obtained main active species (h^+ and $^{\bullet}O_2^-$) reacted with the pollutants to generate the degradation products. Thus, during the photo-catalytic process, the recombined rate of the photo-generated electron–hole pairs was limited to achieve the efficient charge separation, promoting the photocatalytic performance.

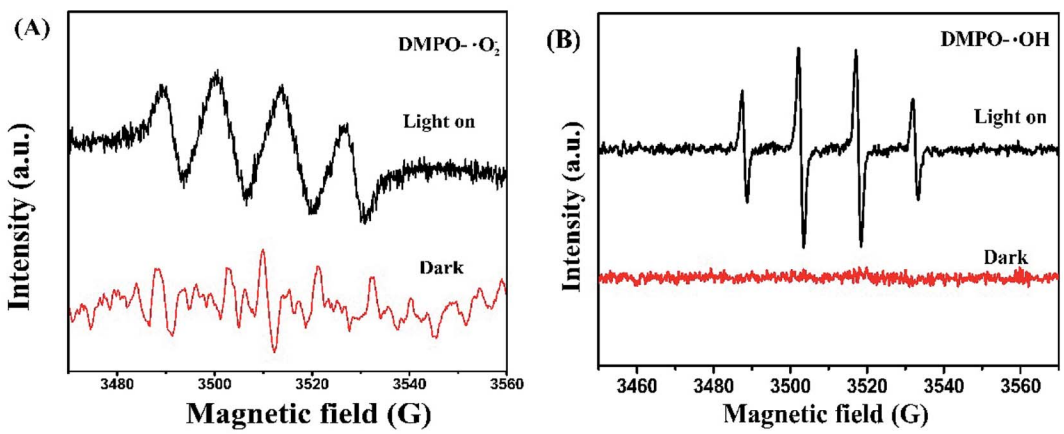

Fig. 9 (A) DMPO spin-trapping ESR spectra of g-C_3N_4/$Bi_{12}O_{17}Cl_2$ (3 wt%) composite in methanol dispersion for DMPO-$^{\bullet}O_2^-$, (B) DMPO spin-trapping ESR spectra of g-C_3N_4/$Bi_{12}O_{17}Cl_2$ (3 wt%) composite deionized water dispersion for DMPO-$^{\bullet}OH$.

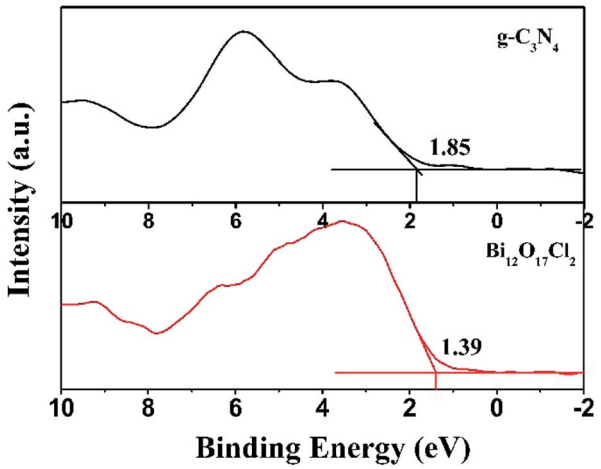

Fig. 10 The VB XPS spectra for g-C_3N_4 and $Bi_{12}O_{17}Cl_2$.

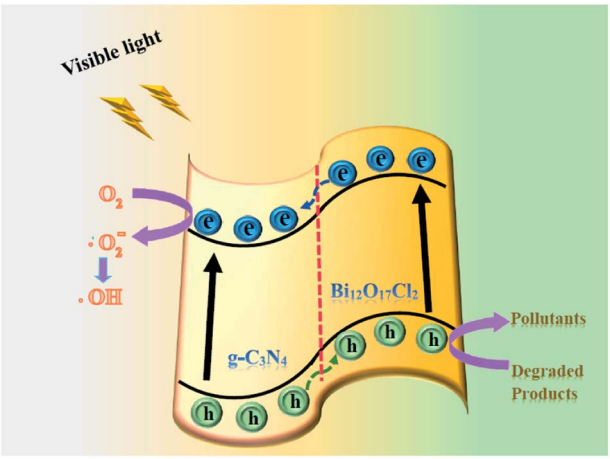

Fig. 11 Separation process of photo-charges over g-C_3N_4/$Bi_{12}O_{17}Cl_2$ under visible light.

4. Conclusions

In conclusion, a novel 2D/2D g-C_3N_4/$Bi_{12}O_{17}Cl_2$ composite photo-catalyst has been successfully fabricated by a one step chemical precipitation method. Compared with pristine g-C_3N_4 and $Bi_{12}O_{17}Cl_2$, g-C_3N_4/$Bi_{12}O_{17}Cl_2$ composites exhibited better photocatalytic performance for the degradation of organic pollutants under visible light irradiation, and kept good recyclability during the photo-degradation process, which could be attributed to the surface-to-surface interfaces between g-C_3N_4 and the $Bi_{12}O_{17}Cl_2$ sheet with a matched energy band structure, promoting the efficient charge separation. The results of the trapping experiment and ESR measurements indicated that $^{\bullet}O_2^-$ and h^+ radicals were the key active species in this reaction. The present work sheds light on the rational design and fabrication of highly efficient photo-catalysts for solving the environmental and energy issues, such as pollutant degradations *etc.*

Conflicts of interest

There are no conflicts of interest to declare.

Acknowledgements

We sincerely acknowledge the financial supported by talent scientific research fund of LSHU (No. 2016XJJ-080), basic research projects of Liaoning Provincial Education Department (L2017LQN004) and NSFC of China (21761132010, 91645114 and 21573256).

References

1 H. Wang, L. Zhang, Z. Chen, J. Hu, S. Li, Z. Wang, J. Liu and X. Wang, *Chem. Soc. Rev.*, 2014, **43**, 5234–5244.
2 M. R. Hoffmann, S. T. Martin, W. Choi and D. W. Bahneman, *Chem. Rev.*, 1995, **95**, 69–96.
3 X. Chen and S. S. Mao, *Chem. Rev.*, 2007, **107**, 2891–2959.
4 L. Ye, Y. Su, X. Jin, H. Xie and C. Zhang, *Environ. Sci.: Nano*, 2014, **1**, 90–112.
5 J. Li, H. Li, G. Zhan and L. Zhang, *Acc. Chem. Res.*, 2017, **50**, 112–121.
6 D. S. Bhachu, S. J. A. Moniz, S. Sathasivam, D. O. Scanlon, A. Walsh, S. M. Bawaked, M. Mokhtar, A. Y. Obaid, I. P. Parkin, J. Tang and C. J. Carmalt, *Chem. Sci.*, 2016, **7**, 4832–4841.
7 S. L. Wang, L. L. Wang, W. H. Ma, D. M. Johnson, Y. F. Fang, M. K. Jia and Y. P. Huang, *Chem. Eng. J.*, 2015, **259**, 410–416.
8 M. Ji, J. Di, Y. Ge, J. Xia and H. Li, *Appl. Surf. Sci.*, 2017, **413**, 372–380.
9 J. Jiang, K. Zhao, X. Xiao and L. Zhang, *J. Am. Chem. Soc.*, 2012, **134**, 4473–4476.
10 L. Ye, K. Deng, F. Xu, L. Tian, T. Peng and L. Zan, *Phys. Chem. Chem. Phys.*, 2012, **14**, 82–85.
11 X. Lin, T. Huang, F. Huang, W. Wang and J. Shi, *J. Phys. Chem. B*, 2006, **110**, 24629–24634.
12 C. Y. Wang, X. Zhang, X. N. Song, W. K. Wang and H. Q. Yu, *ACS Appl. Mater. Interfaces*, 2016, **8**, 5320–5326.
13 B. Yin, Z. Fang, B. Luo, G. Zhang and W. Shi, *Catal. Lett.*, 2017, **147**, 2167–2172.
14 C. Y. Wang, X. Zhang, H. B. Qiu, W. K. Wang, G. X. Huang, J. Jiang and H. Q. Yu, *Appl. Catal., B*, 2017, **200**, 659–665.
15 X. Xiao, J. Jiang and L. Zhang, *Appl. Catal., B*, 2013, **142–143**, 487–493.
16 W. J. Ong, L. L. Tan, Y. H. Ng, S. T. Yong and S. P. Chai, *Chem. Rev.*, 2016, **116**, 7159–7329.
17 Y. Wang, X. Wang and M. Antonietti, *Angew. Chem., Int. Ed.*, 2012, **51**, 68–89.
18 Z. Zhao, Y. Sun and F. Dong, *Nanoscale*, 2015, **7**, 15–37.
19 Q. Li, N. Zhang, Y. Yang, G. Wang and D. H. L. Ng, *Langmuir*, 2014, **30**, 8965–8972.
20 X. J. Wang, Q. Wang, F. T. Li, W. Y. Yang, Y. Zhao, Y. J. Hao and S. J. Liu, *Chem. Eng. J.*, 2013, **234**, 361–371.
21 S. Kumar, T. Surendar, A. Baruah and V. Shanker, *J. Mater. Chem. A*, 2013, **1**, 5333–5340.

22 C. Pan, J. Xu, Y. Wang, D. Li and Y. Zhu, *Adv. Funct. Mater.*, 2012, **22**, 1518–1524.
23 L. Ge, F. Zuo, J. Liu, Q. Ma, C. Wang, D. Sun, L. Bartels and P. Feng, *J. Phys. Chem. C*, 2012, **116**, 13708–13714.
24 R. Yin, Q. Luo, D. Wang, H. Sun, Y. Li, X. Li and J. An, *J. Mater. Sci.*, 2014, **49**, 6067–6073.
25 Y. Ma, Y. Bian, P. Tan, Y. Shang, Y. Liu, L. Wu, A. Zhu, W. Liu, X. Xiong and J. Pan, *J. Colloid Interface Sci.*, 2017, **497**, 144–154.
26 H. Li, J. Liu, W. Hou, N. Du, R. Zhang and X. Tao, *Appl. Catal., B*, 2014, **160–161**, 89–97.
27 J. X. Sun, Y. P. Yuan, L. G. Qiu, X. Jiang, A. J. Xie, Y. H. Shen and J. F. Zhu, *Dalton Trans.*, 2012, **41**, 6756–6763.
28 L. Ye, J. Liu, Z. Jiang, T. Peng and L. Zan, *Appl. Catal., B*, 2013, **142–143**, 1–7.
29 N. Tian, Y. Zhang, C. Liu, S. Yu, M. Li and H. Huang, *RSC Adv.*, 2016, **6**, 10895–10903.
30 C. Zhou, C. Lai, P. Xu, G. Zeng, D. Huang, Z. Li, C. Zhang, M. Cheng, L. Hu, J. Wan, F. Chen, W. Xiong and R. Deng, *ACS Sustainable Chem. Eng.*, 2018, **6**, 6941–6949.
31 C. Bi, J. Cao, H. Lin, Y. Wang and S. Chen, *Mater. Lett.*, 2016, **166**, 267–270.
32 C. Bi, J. Cao, H. Lin, Y. Wang and S. Chen, *Appl. Catal., B*, 2016, **195**, 132–140.
33 L. Yao, L. Shi and F. Wang, *Mater. Res. Express*, 2018, **5**, 045042.
34 K. Kobayakawa, Y. Murakami and Y. Sato, *J. Photochem. Photobiol., A*, 2005, **170**, 177–179.
35 L. Shi, J. Ma, L. Yao, L. Cui and W. Qi, *J. Colloid Interface Sci.*, 2018, **519**, 1–10.
36 X. Y. Chen, H. S. Huh and S. W. Lee, *J. Solid State Chem.*, 2007, **180**, 2510–2516.
37 L. Shi, F. Wang, J. Zhang and J. Sun, *Ceram. Int.*, 2016, **42**, 18116–18123.
38 Y. Kang, Y. Yang, L. C. Yin, X. Kang, G. Liu and H. M. Cheng, *Adv. Mater.*, 2015, **27**, 4572–4577.
39 Y. Zhou, L. Zhang, W. Huang, Q. Kong, X. Fan, M. Wang and J. Shi, *Carbon*, 2016, **99**, 111–117.
40 S. Cao, Q. Huang, B. Zhu and J. Yu, *J. Power Sources*, 2017, **351**, 151–159.
41 L. Shi, L. Liang, F. Wang, M. Liu, K. Chen, K. Sun, N. Zhang and J. Sun, *ACS Sustainable Chem. Eng.*, 2015, **3**, 3412–3419.
42 F. Chang, X. Wang, J. Luo, J. Wang, Y. Xie, B. Deng and X. Hu, *J. Mol. Catal. A: Chem.*, 2017, **427**, 45–53.
43 G. He, C. Xing, X. Xiao, R. Hu, X. Zuo and J. Nan, *Appl. Catal., B*, 2015, **170–171**, 1–9.
44 H. Huang, K. Xiao, Y. He, T. Zhang, F. Dong, X. Du and Y. Zhang, *Appl. Catal., B*, 2016, **199**, 75–86.
45 L. Zhang, Y. Zhang, R. Shi, S. Bao, J. Wang, A. Amini, B. N. Chandrashekar and C. Cheng, *Materials Today Energy*, 2017, **5**, 91–98.
46 Y. Yang, Y. Guo, F. Liu, X. Yuan, Y. Guo, S. Zhang, W. Guo and M. Huo, *Appl. Catal., B*, 2013, **142–143**, 828–837.
47 L. Shi, L. Liang, J. Ma, Y. N. Meng, S. F. Zhong, F. X. Wang and J. M. Sun, *Ceram. Int.*, 2014, **40**, 3495–3502.
48 M. Zhang, C. Bi, H. Lin, J. Cao and S. Chen, *Mater. Lett.*, 2017, **191**, 132–135.
49 J. Xu, Y. Hu, C. Zeng, Y. Zhang and H. Huang, *J. Colloid Interface Sci.*, 2017, **505**, 719–727.
50 L. Shi, L. Liang, J. Ma, F. X. Wang and J. M. Sun, *Dalton Trans.*, 2014, **43**, 7236–7244.
51 C. Hu, T. Peng, X. Hu, Y. Nie, X. Zhou, J. Qu and H. He, *J. Am. Chem. Soc.*, 2010, **132**, 857–862.
52 A. R. Upreti, Y. Li, N. Khadgi, S. Naraginti and C. Zhang, *RSC Adv.*, 2016, **6**, 32761–32769.
53 J. Ma, L. Shi, L. Yao, Z. Wang, C. Lu, W. Qi and D. Su, *ChemistrySelect*, 2017, **2**, 8535–8540.
54 S. He, Q. Rong, H. Niu and Y. Cai, *Chem. Commun.*, 2017, **53**, 9636–9639.
55 S. G. Kumar and K. S. R. K. Rao, *RSC Adv.*, 2015, **5**, 3306–3351.
56 N. Wang, L. Shi, L. Yao, C. Lu, Y. Shi and J. Sun, *RSC Adv.*, 2018, **8**, 537–546.